SANDIA REPORT

SAND2002-0526
Unlimited Release
Printed March 2002

3-D CAVERN ENLARGEMENT ANALYSES

Brian L. Ehgartner, Underground Storage Technology Department
Steven R. Sobolik, Geomechanics Department

Prepared by
Sandia National Laboratories
Albuquerque, New Mexico 87185 and Livermore, California 94550

Sandia is a multiprogram laboratory operated by Sandia Corporation, a Lockheed Martin Company, for the United States Department of Energy under Contract DE-AC04-94AL85000.

Issued by Sandia National Laboratories, operated for the United States Department of Energy by Sandia Corporation.

Available to DOE and DOE contractors from
U.S. Department of Energy
Office of Scientific and Technical Information
P.O. Box 62
Oak Ridge, TN 37831

Telephone: (865)576-8401
Facsimile: (865)576-5728
E-Mail: reports@adonis.osti.gov
Online ordering: http://www.doe.gov/bridge

Available to the public from
U.S. Department of Commerce
National Technical Information Service
5285 Port Royal Rd
Springfield, VA 22161

Telephone: (800)553-6847
Facsimile: (703)605-6900
E-Mail: orders@ntis.fedworld.gov
Online order: http://www.ntis.gov/ordering.htm

SAND2001-0526
Unlimited Release
Printed April 2001

Distribution
Category UC-126

3-D Cavern Enlargement Analyses

Steven R. Sobolik
Geomechanics Department

Brian L. Ehgartner
Underground Storage Technology Department

Sandia National Laboratories
P.O. Box 5800
Albuquerque, NM 87185-0706

Abstract

Three-dimensional finite element analyses simulate the mechanical response of enlarging existing caverns at the Strategic Petroleum Reserve (SPR). The caverns are located in Gulf Coast salt domes and are enlarged by leaching during oil drawdowns as fresh water is injected to displace the crude oil from the caverns. The current criteria adopted by the SPR limits cavern usage to 5 drawdowns (leaches). As a base case, 5 leaches were modeled over a 25 year period to roughly double the volume of a 19 cavern field. Thirteen additional leaches where then simulated until caverns approached coalescence.

The cavern field approximated the geometries and geologic properties found at the West Hackberry site. This enabled comparisons are data collected over nearly 20 years to analysis predictions. The analyses closely predicted the measured surface subsidence and cavern closure rates as inferred from historic well head pressures. This provided the necessary assurance that the model displacements, strains, and stresses are accurate. However, the cavern field has not yet experienced the large scale drawdowns being simulated. Should they occur in the future, code predictions should be validated with actual field behavior at that time.

The simulations were performed using JAS3D, a three dimensional finite element analysis code for nonlinear quasi-static solids. The results examine the impacts of leaching and cavern workovers, where internal cavern pressures are reduced, on surface subsidence, well integrity, and cavern stability. The results suggest that the current limit of 5 oil drawdowns may be extended with some mitigative action required on the wells and later on to surface structure due to subsidence strains. The predicted stress state in the salt shows damage to start occurring after 15 drawdowns with significant failure occurring at the 16^{th} drawdown, well beyond the current limit of 5 drawdowns.

Acknowledgments

The authors would like to acknowledge the continued support of Gerard Berndsen, DOE SPRPMO, who initiated this study. Also, the discussions and inputs of Ray E. Finley and Larry S. Costin of Sandia, were of great benefit.

Contents

Figures

Tables

1.0 Introduction

The efficient utilization of SPR caverns requires a clear understanding of the geotechnical consequences associated with oil drawdowns. Drawdowns are typically accomplished by injecting water into a cavern which displaces the crude oil out of the cavern. The use of raw or fresh water leaches salt which creates additional underground volume, but smaller pillars of salt in between caverns. Thin pillars of salt separating caverns could eventually lead to cavern instability or excessive subsidence.

The SPR currently limits the size of its caverns on the basis of the ratio between the pillar width (P) and the diameter of the cavern (D). The minimum allowed P/D ratio is 1.78, which allows up to 5 oil drawdowns in most cases. The P/D ratio was established during the startup of the program, approximately 20 years ago, and is believed to be conservative (Ehgartner, 2000). The criteria not only controls the number of drawdowns, but also constrains cavern development. Enlargement of existing caverns through leaching is a relatively quick and economic way of increasing storage space when compared to the alternative(s) of adding caverns to an existing field or creating a new cavern field.

The benefits of increasing the allowable P/D ratio are increased cavern utilization by allowing for more oil drawdowns and developing existing cavern storage volume. There are however consequences associated with larger caverns. A larger cavern creeps faster and requires more frequent bleed-downs, and hence additional brine disposal, to control cavern pressure. Additional subsidence results from larger caverns, which could adversely affect surface structures and cavern wells. The purpose of this report is to quantify the consequences of leaching SPR caverns through 3-D finite element analyses.

2.0 Problem Description

2.1 Cavern Geometry

The cavern geometries[1] and geology are based on caverns at SPR West Hackberry as shown in Figure 1. The Phase II caverns are approximately 2500 ft deep at the roof, stand approximately 2000 ft. high, and are nominally 200 ft in diameter. The caverns are spaced at approximately 750 ft apart. The West Hackberry field contains 22 SPR caverns and a number of smaller industrial caverns. A layout of the site is shown in Figure 2.

The finite element model used for this study includes the domal stratigraphy of salt, a 400 ft thick caprock and 1000 ft of overburden consistent with the general geology at West Hackberry. Since the caverns are located in the central portion of the dome, symmetry planes can be used in the model. The model simulates 19 caverns in a systematic pattern

[1] Note: Both metric and English units are used in this report in convention with the discipline being discussed. Conversions are: 1ft = 0.3048 m, 145 psi = 1 Mpa.

with equal spacing and uniform cavern size and geometry. The location of the symmetry planes are illustrated in Figure 3a and the generalized model showing stratigraphy in Figure 3b.

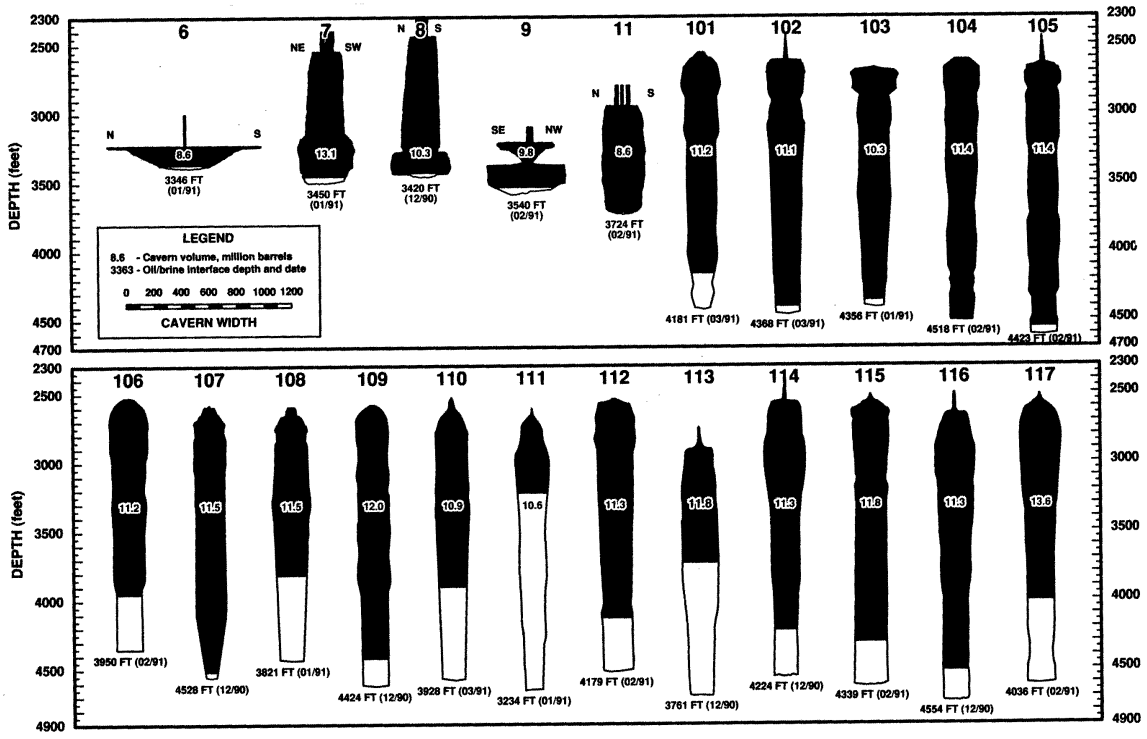

Figure 1. West Hackberry Caverns

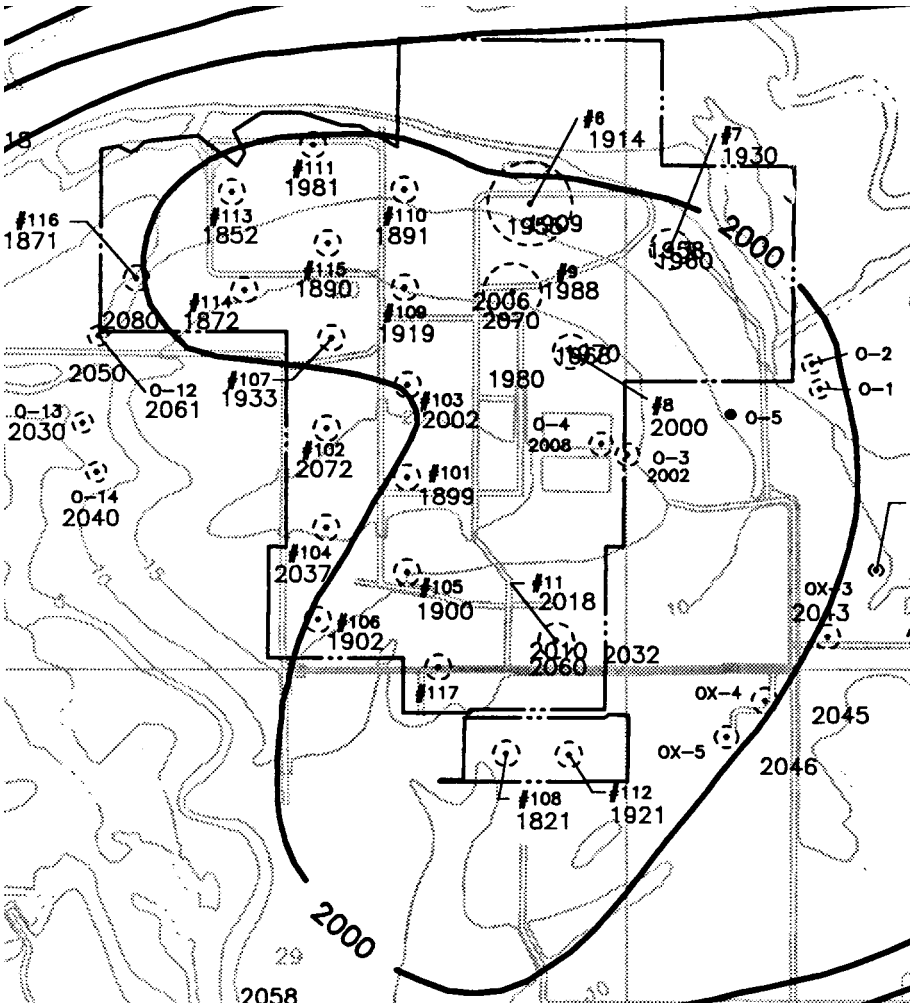

Figure 2. Layout of West Hackberry Field showing location of SPR and industry caverns. Also shown is 2000 ft contour elevation to top of salt.

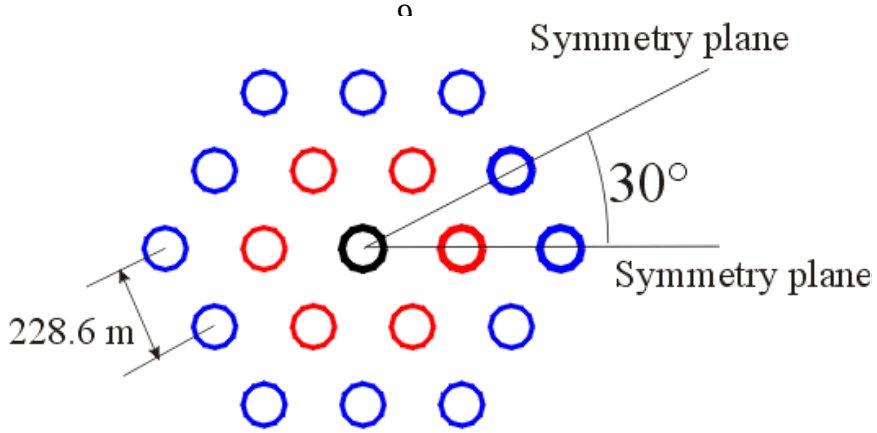

(a) SPR 19 cavern layout

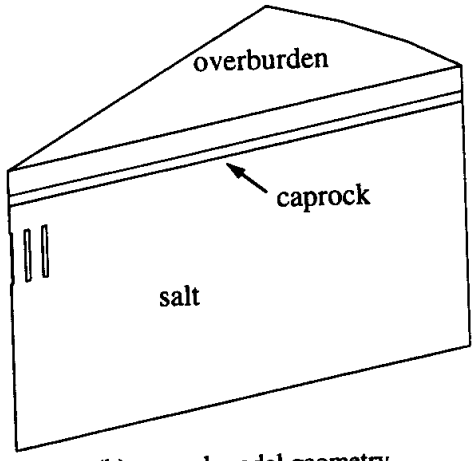

(b) general model geometry

Figure 3. Idealized cavern spacing and model showing symmetry planes.

2.2 Model History

The analysis history simulated caverns that were leached to full size over a one year period, filled with oil, and then permitted to creep for 20 years to approximate the current age of the caverns at most sites, in particular the Phase II caverns at West Hackberry. At 20 years and subsequently every 5 years, the caverns were leached by deleting elements along the wall of the caverns to result in an increased volume of 15 percent for each leach as shown in Table 1. Leaching was assumed to occur uniformly along the entire height of the cavern and not permitted in the floor or roof of the caverns. A 5 year period between

leaching allows the stress state in the salt to return to a steady-state condition as will be evidenced in the predicted closure rates predicted. Thus the predicted stress states are not expected to be sensitive to the 5 year leach frequency used in the analyses.

Table 1. Drawdown Properties

Drawdown	Time of Leach (yrs)	Cavern Vol. (MMB)	Cavern Diameter (ft)	Min. Pillar Width (ft)	P/D Ratio
1	20	11.2	200	550	2.8
2	25	12.9	214	536	2.5
3	30	14.8	230	520	2.3
4	35	17.0	247	503	2.0
5	40	19.6	265	486	1.8
6	45	22.5	284	466	1.6
7	50	25.9	304	446	1.5
8	55	29.8	326	424	1.3
9	60	34.3	350	400	1.1
10	65	39.4	375	375	1.0
11	70	45.3	402	348	0.9
12	75	52.1	431	319	0.7
13	80	59.9	463	287	0.6
14	85	68.9	496	254	0.5
15	90	79.2	532	218	0.4
16	95	91.1	571	179	0.3
17	100	104.8	612	138	0.2
18	105	120.5	656	94	0.1

The pressure condition applied to the cavern was based on a wellhead pressure of 975 psi, which is considered typical for West Hackberry caverns operating at normal pressure, and assumed caverns that are full of oil (a pressure gradient of 0.37 psi/ft of depth). In these analyses, a constant pressure is applied over time and pressure drops are periodically included to simulate times when caverns are operated at lower than normal pressures and during workover conditions (0 psi wellhead). An analysis of cavern pressures at West Hackberry from 1990 to 2000 shows that a cavern is pressurized within its normal operating range 90 percent of the time and at lower pressures for 10 percent of the time. Rather than complicating the analyses, low pressure conditions are simulated at the extreme end of the less than normal range (0 psi wellhead) to account for workover conditions, which in general occur at a frequency of every 5 years in conjunction with the Cavern Integrity Test program. This abrupt pressure drop will induce the greatest potential for damage. For simulation purposes, the pressure drop to 0 psi for each cavern lasts for 3 months, which accounts for 5 percent of time over a 5 year period. The duration of the workover may be slightly longer than commonly encountered in the field, but is chosen to provide an adverse condition and closely simulate actual subsidence measurements.

To approximate actual field conditions, not all caverns are in workover mode at the same time. The central cavern in the field is the first cavern in the workover sequence starting at one year after initial cavern leaching and continuing every 5 years until the end of the simulations. This scheme places the central cavern in workover mode one year after each cavern leach. Because of mesh symmetry, workover pressures must be applied to the entire second ring of caverns at the same time. This results in the 6 neighboring caverns at low pressure starting one year after each workover of the central cavern. This condition enables the web of salt between adjacent caverns in workover mode to be examined for stability. As well, the webs of salt between caverns in workover mode and those under normal operating pressures can be studied. The workover sequence continues with the outer ring of caverns being subject to workover pressures one year after the second ring, followed by the third ring of caverns (on the 30° symmetry plane) in workover mode a year later. The convention used to discuss these rings of caverns in the model, it to simply refer to them as caverns 1, 2 and 3 from the inner to outer most ring, with cavern 4 located on the 30° symmetry plane.

2.3 Structural Model

The finite element code used in the present calculations, JAS3D (Blandford, 1998), uses an eight-node hexahedral Lagrangian uniform strain element with hourglass stiffness to control zero energy modes. A nonlinear conjugate gradient method is used to solve the nonlinear system of equations. This efficient solution scheme is considerably faster than the direct solvers which are used in most commercial codes and is a product of decades of research and development into nonlinear large strain finite element analyses.

The 3D finite element model used in the present calculations is shown in detail in Figure 4. The model was constructed of 8-node bricks consists of 69300 nodes and 61773 elements. Because of vertical symmetry, only one-twelfth of the model is represented by the finite element mesh is illustrated in the Figure 4. Figure 4 (bottom) shows a plan view close-up of the model domain immediately surrounding the 4 caverns included in the finite element mesh. Each ring (dark color) represent those elements of salt that will become cavern during subsequent leaches. The rings represent 15 percent increase in cavern volume. Each cavern is surrounded by 18 rings of elements to account for up to 18 total leaches following initial construction. Note that the full complement of leaches results in almost full coalescence of adjacent caverns.

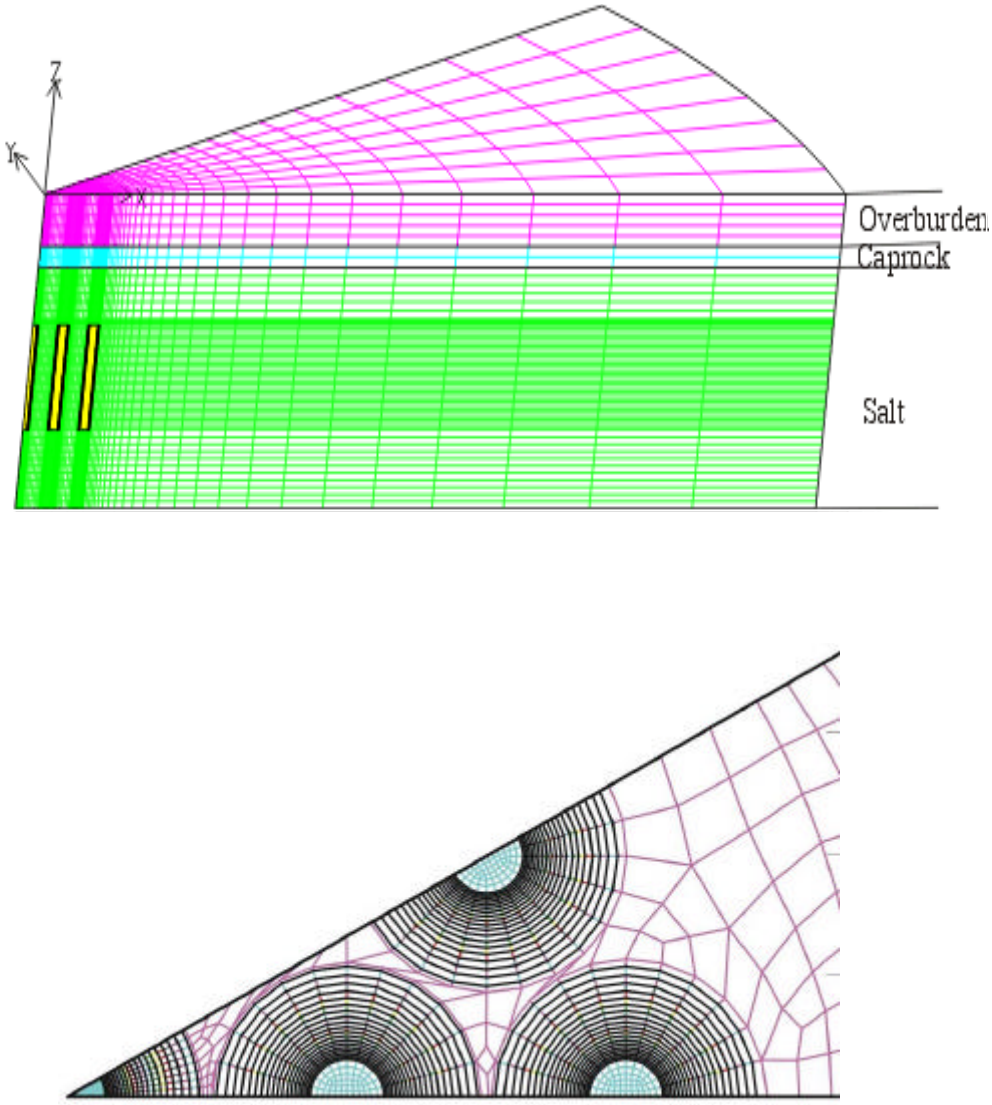

Figure 4. Finite element mesh (top) with cross-section through caverns (bottom).

Displacements were constrained in the direction normal to this plane and all outer vertical surfaces of the mesh. The far field boundary (curved boundary) is 6000 ft from the center cavern, a distance representing the edge of the dome.

Gravitational body forces were applied to the model. To ensure initial equilibrium, elevation-dependent initial stresses are applied to each element in the model based on the density of the overburden, caprock, and salt. In the elastic materials (overburden and caprock), the vertical stress component at a given location was applied based on the weight of the material above that point. The horizontal component was applied to be

consistent with a vertically loaded elastic material in equilibrium. Under these load conditions, the resulting ratio of horizontal to vertical stress components is defined as follows:

$$\frac{s_h}{s_v} = \frac{v}{1-v}$$

where v is the Poisson's ratio of the material. For the salt, an initial stress state was assumed in which the vertical and horizontal stress components are equal to the weight of the overlying material (lithostatic).

2.4 Thermal Model

The finite element model included a depth-dependent temperature gradient which starts at 80 °F at the surface and increased at the rate of 0.012 °F/ft. The temperature distribution is important because the creep response of the salt is temperature dependent. Radial temperature gradients due to cavern cooling were not considered in these calculations. Previous 2D cavern studies have shown the predicted cavern deformation to be insensitive to radial thermal gradients developed by cooling effects of the cavern product (Hoffman, 1992).

2.5 Constitutive Models and Material Properties

The geomechanical properties for West Hackberry salt were derived through testing of salt core collected from boreholes (Wawersik and Zeuch, 1984). The creep constitutive model considered only secondary or steady-sate creep. The creep strain rate is determined from the effective stress as follows:

$$\dot{e} = A\left(\frac{s}{m}\right)^n \exp\left(-\frac{Q}{RT}\right)$$

where

$\dot{e}$ is the creep strain rate,

s is the effective or von Mises stress,

μ is the shear modulus, $E/2(1+\nu)$,

T is absolute temperature,

A and n are constants determined from fitting the model to creep data,

Q is the effective activation energy,

R is the universal gas constant.

The elastic and creep constants used for the salt are given in Table 2. The overburden and caprock were modeled as elastic materials without a failure criterion. The properties assume a homogeneous material and the modulus was reduced from those measured in the laboratory to account for large scale discontinuities and fracturing of the caprock (Preece and Foley, 1984). The modulus of salt listed in Table 2 has been reduced from its laboratory value. Using the reduced modulus has been shown to simulate the transient response of salt around underground excavations (Morgan and Krieg, 1990). The structure factor is known to vary for salts (Munson, 1998) and the limited creep testing of SPR salts (Wawersik and Zeuch, 1984) showed considerable variability in creep rates (up to an order of magnitude difference). Therefore, the structure factor was varied to best match the measured closure and subsidence rates in Section 3.1. In addition to using the typical structure factor (1.25×10^{15} 1/sec), the typical value was reduced by a factor of 5 to simulate stiffer salt, which was found to be more vulnerable to damage. The stability results presented in this report are based on the stiffer structure factor which represents a lower bound stiffness, but an upper bound for potential damage.

Table 2. Structural Properties of Overburden, Caprock, and Salt

Materials	Young's Modulus, E (Gpa)	Poisson's Ratio, ν	Density, ρ kg/m^3	Structure Factor, A (1/sec)	Stress Exponent n	Activation Energy, Q (kcal/mole)
Overburden	0.1	.33	1874	--	--	--
Caprock	7.0	.29	2500	--	--	--
Salt	2.48	.25	2300	.25 to 1.25 x 10^{15}	4.9	12.0

2.6 Structural Stability of Rock Salt

This study evaluated the potential for damage to or around the caverns based on two criteria: dilatant damage and tensile failure. Dilatancy is considered the onset of damage to the salt resulting in potentially large increases in permeability. The dilatancy criterion was taken from the literature which shows a very consistent ratio of 0.25 between the second invariant of the deviatoric stress and the first invariant of stress.

The dilatant damage criterion is used to delineate potential zones of dilatancy in the salt formation surrounding the storage facility. Dilatancy is attributed to microfracturing or changes in the pore structure of the salt, resulting in an increase in permeability. The

potential for dilatant damage is defined by a "damage" safety factor (D) which is expressed as follows:

$$D = \frac{I_1}{4\sqrt{J_2}}$$

where J_2 is the second invariant of the deviatoric stress tensor, and I_1 is the first invariant of the stress tensor ($I_1 = 3s_m$, where s_m is the mean stress). When D is equal to or less than one, the shear stresses in the salt are large compared to the mean stress and the potential for dilatant behavior is high (Speirs, 1988; Van Sambeek 1993). Hunsche (1992) suggests that dilatancy is linked to creep rupture in that as the rock salt dilates, its structure loosens and may fail after some time due to creep rupture. A summary of laboratory tests on SPR and other rock salts along with failure and damage criteria are compiled in Tavares (1994). Based on an evaluation of the SPR rock mechanics test data in terms of the above criteria, failure occurs when the damage safety factor is less than 0.6.

For the purposes of these analyses, the tensile strength of the salt was conservatively assumed to be zero. Tensile cracking in rock salt tends to initiate perpendicular to the largest tensile stress in the rock. The potential for tensile failure exists if the maximum principal stress is tensile or numerically positive.

It should be clearly stated that the above dilatation criteria is not used in the present study to quantify damage, but merely to identify regions with a high potential for damage even though the estimates are considered conservative for the reasons stated above. This criteria identifies regions where the deviatoric stress is high and the mean stress is low, a stress state conducive to dilation. No comprehensive constitutive model exists at this time which can predict damage evolution in a reasonable computation time for a 3D problem of this size. Hence, the post-processed dilatation criteria was used as a conservative engineering approach to estimate possible regions of salt dilation. Much can be inferred from this criterion. For example, if the dilatant damage safety factor is decreasing with time, it can be concluded that the potential for damage is increasing. Hence, salt healing (a reduction in dilatancy) is not likely to occur. Second, if the predicted damage is growing in both size and magnitude, then the damaged region (fracture or dilation) will continue to grow. Similarly, if a tensile region is predicted to be growing in both size and magnitude, the resulting fractures, although not explicitly modeled, should also grow.

2.7 Allowable Strains for Well and Surface Structures

The physical presence of wells and surface structures are not included in the finite element model, but the potential for ground deformation to damage these structures can be conservatively estimated by assuming that they will deform according to the predicted ground strains. At wells locations, subsidence will primarily induce elongation of the axis of the well. Under these conditions, the cemented annulus of the wells may crack forming a horizontal tensile fracture that my extend around the wellbore. This may not result in vertical fluid migration along the casing, but could permit horizontal flow. This may be a

vulnerability, especially in the caprock, where acidic ground waters may gain access to the steel casing and corrode it. More extensive damage could heavily fracture the cement which could result in a loss of well integrity in that leakage could occur from the cavern along the outside of the casing.

The allowable strain for purposes of this report is assumed to be 2 millistrains in compression and 0.2 millistrains in tension. This would be typical of a cement with a compressive strength in the range from 2500 to 5000 psi (Thorton and Lew, 1983). The benefit of the steel casings in reinforcing the strength of the cement, especially under elongation, is not accounted for in this simplistic evaluation.

Structural damage on the surface is typically caused by large accumulated surface strains caused by surface subsidence. These strains can cause distortion, cracking, and failure of buildings, pipelines, roads, bridges, and other infrastructure. Surface strains will accumulate in structures over time, which increases the possibility of damage in older facilities. Subsidence strains tend to be compressive in the central portion of the subsided area and become tensile in nature for areas farther removed. Some guidance and solutions are available to evaluate the predicted surface strains. These criteria vary from country to country, possibly due to different building codes and structural materials. Some examples of allowable strains are presented in Table 3 (Peng, 1985).

Table 3. Allowable Mining Ground Strains (millistrains)

Country	Compression	Tension	Application
China	--	2	--
England	1	--	--
France	1 to 2	0.5	Pipelines
Germany	0.6	0.6	--
Japan	0.5	0.5	Concrete foundations
Poland	1.5	1.5	--
Soviet Union	2 to 4	2 to 4	--

The criteria varies in some countries depending on application and criteria for shear strains have not been found, perhaps because they are a minor influence. For purposes of this paper, the allowable strain is taken to be 1 millistrain for both compression and tension. In practice, allowable strain limits for a structure are design specific and should be examined on a case-by-case basis.

3.0 Analysis Results

3.1 Comparison to Field Data

In order to validate whether the 3-D model is predicting stresses, strains, and deformations correctly, comparisons can be made to field data collected at West Hackberry. Two types of data have been collected for the SPR- subsidence and cavern pressures at the wellhead.

At West Hackberry subsidence data exists back to January 1983 at about the time when many of the caverns in the field were being developed. The subsidence surveys were performed on a yearly basis or so. The surveys measure surface elevations over the caverns and at other selected locations of interest to the SPR. Subsidence is calculated as the difference or change between survey elevations.

For purposes of comparing to model predictions, only subsidence measurements over SPR caverns constructed no earlier than 1 year prior to the first subsidence survey and found in the interior of the field (with at least 5 or more immediate neighboring caverns) were considered for comparison to the subsidence predictions over the center cavern of the model. The measured subsidence over caverns meeting these criteria (Caverns 107, 109, 110, 114, and 115) is shown in Figure 5 along with the predicted response.

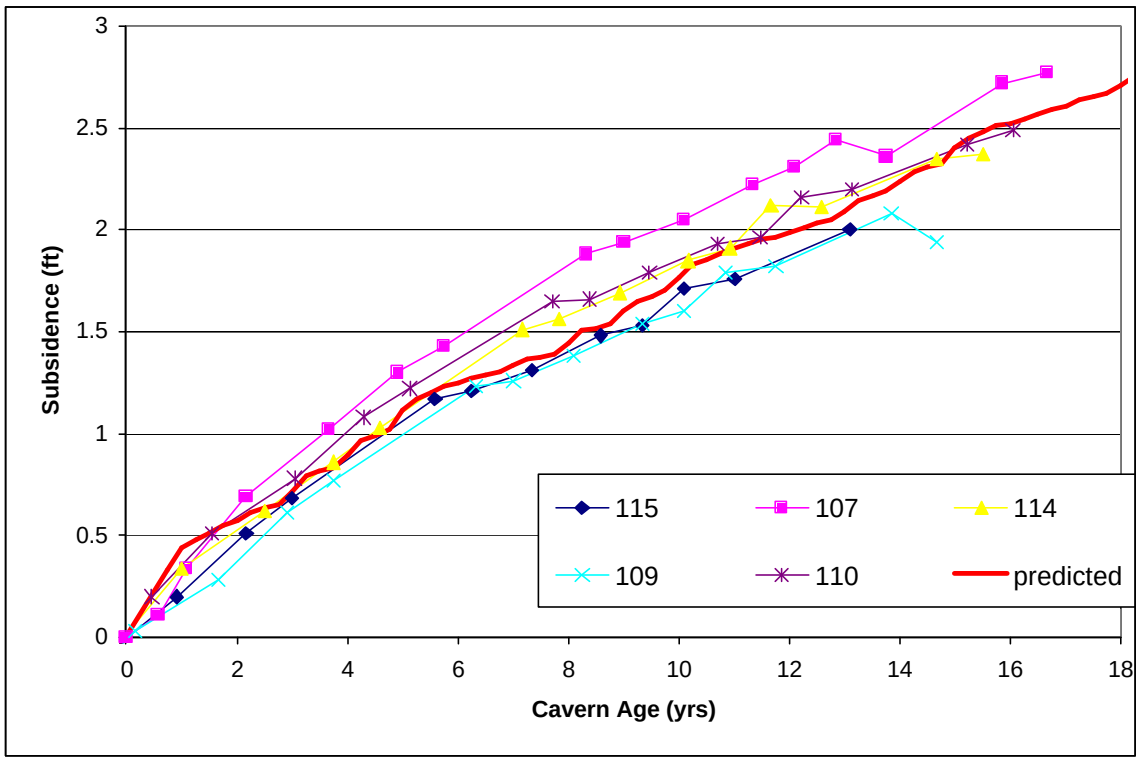

Figure 5. Measured and predicted surface subsidence over West Hackberry.

Cavern closure rates were calculated from wellhead data collected on a daily basis over the last 10 years. In order to calculate closure rates, the compressibility of the fluid in the caverns and the thermal history was needed. To evaluate the thermal contribution to the measured wellhead pressures, the thermal model in Caveman version 3 (Ballard and Ehgartner, 2000) was used. As well, the information on fluid transfers, etc. as found in Caveman was used. Since cavern pressurization rates and hence closure rates are a strong

function of the operating pressure of the cavern, only data within the normal operating range of the cavern was used. This represents the majority of data collected and is needed for comparison to the model results that assume a constant cavern pressure based on the average wellhead pressure over the normal operating range.

The predicted and measured subsidence and closures rates are shown in Figure 6 to agree reasonably close with each other. The predictions for both closure and subsidence rates are within the scatter measured, thus providing some confidence that the impact of leaching on the cavern field will be adequately predicted.

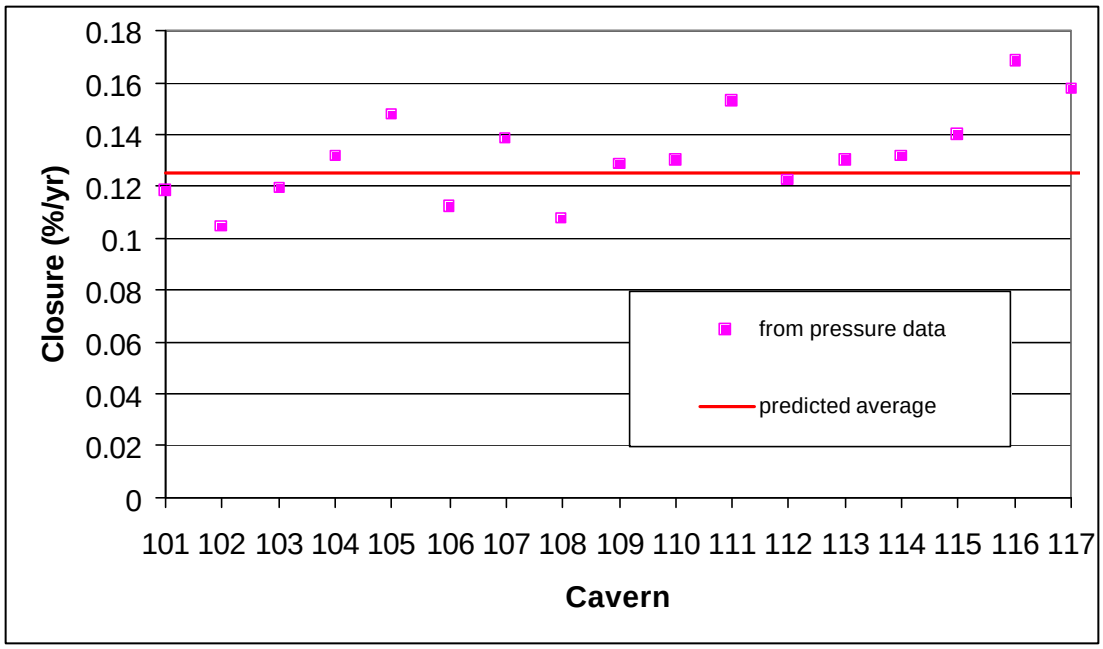

Figure 6. Cavern closure rates at normal operating pressure inferred from wellhead pressure data using Caveman version 3 and predicted from the 3-D model.

3.2 Cavern Deformation

Creep closure is known to decrease cavern volume over time. The flow of salt can be illustrated by displacements vectors. The deformed cavern shapes and displacement vectors are shown in Figure 7 at 45 years, immediately before the 6th leach. The salt flows are primarily downward near the roofs of the caverns, upward near the floors, and laterally in the pillars of salt. Over time, the outer caverns tend to shift inward. The offset is most

notable near the bottom of the outer caverns. The greatest displacements occur in the floors of the caverns. The vertical displacements are quantified in Figure 8, immediately following the 5th leach. The displacements in the floor are predicted to be slightly greater than twice that predicted in the roof of the caverns.

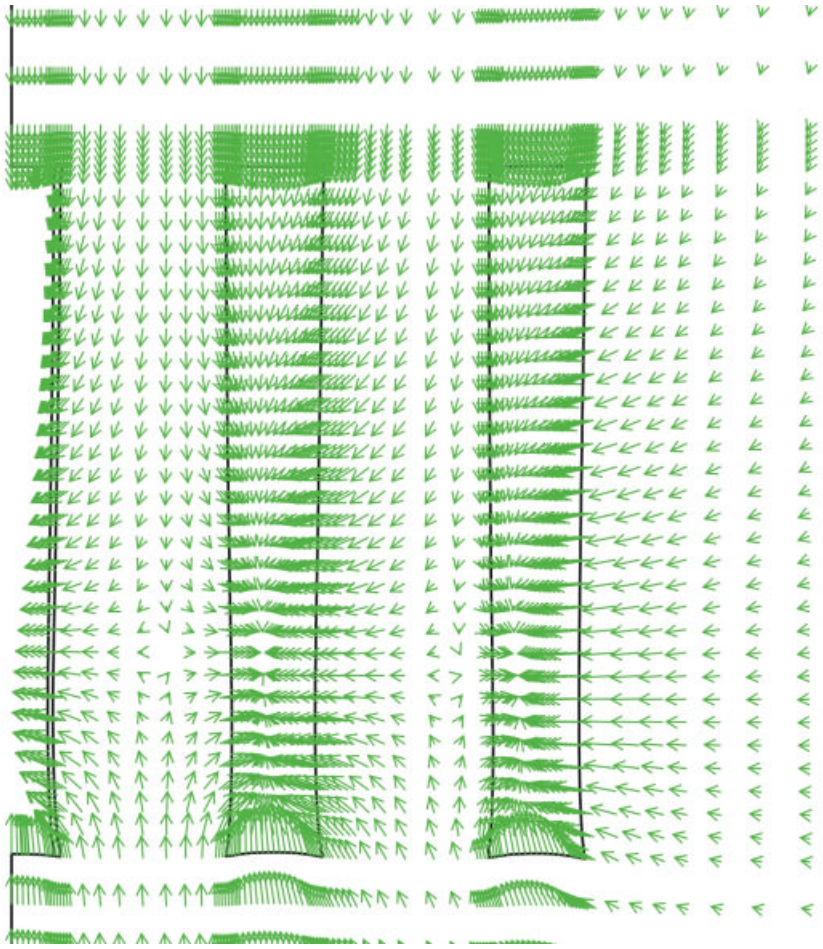

Figure 7. Displacement Vectors at 45 yrs, immediately before the 6th leach

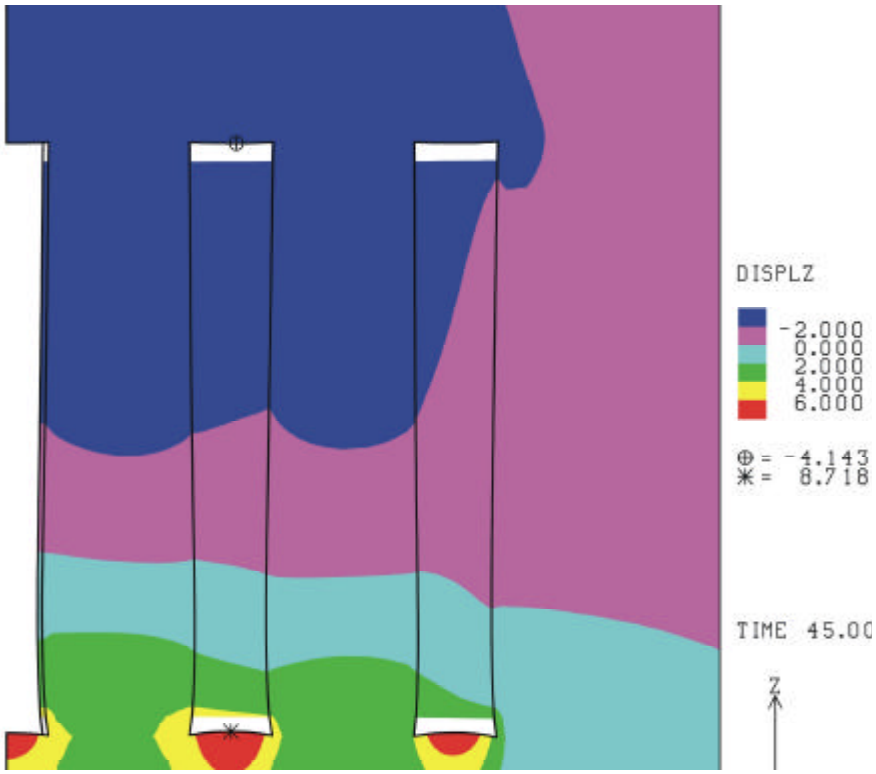

Figure 8. Vertical Displacements at 45 yrs, immediately before the 6th leach.

3.3 Storage Loss

Figure 9 shows the storage volume of the cavern field normalized to the caverns initial volume prior to and following each. Thus, for each leach starting at 20 years and continuing every 5 years thereafter, the cavern volume increases 15 %. Of interest in Figure 9 is the lack of large increases in the normalized closure rate due to cavern leaching. The inner most caverns close at the same rate as the outer caverns.

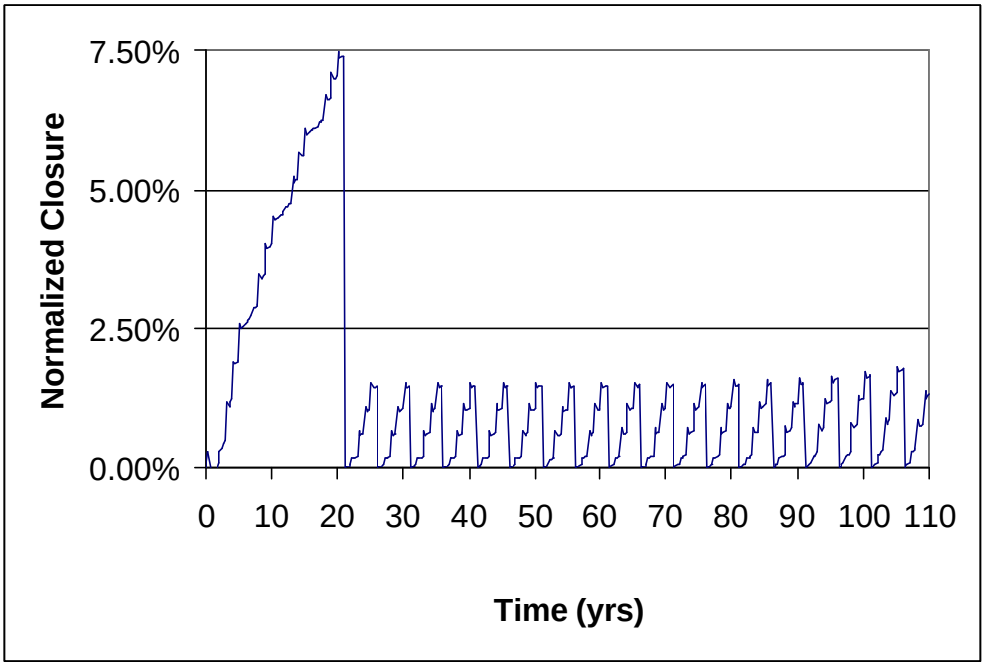

Figure 9. Volumetric closure normalized to cavern volume before and immediately after each leach.

3.4 Subsidence

The subsidence over the center cavern is plotted as a function of time in Figure 10. The subsidence rate slowly increases with time as a result of the larger caverns. As discussed above, the closure rates of the caverns, as expressed as a percentage of cavern volume, do not significantly increase with time. Therefore, the subsidence rates are largely related to cavern volume, and the upward trend in subsidence magnitude and rates over time does not reflect accelerating creep as much as increased cavern volume. The subsidence magnitudes will be problematic at some point due to increased flood potential, where wellhead elevations range from 4 to 17 ft above mean sea level at West Hackberry (Bauer, 1999).

Figure 11 shows the vertical ground displacements immediately before the first and following the 5th leach. The region of subsidence influence is predicted to extend to greater distances over time. The surface subsidence is similar in magnitude to that at the top of salt subsidence, but the disparity increases near the center of the cavern field. The difference between surface and top of salt subsidence results in well strains, which are discussed in the next section, but are predicted here to be greater over the central portions of the cavern field. Figure 12 shows the predicted surface subsidence troughs at selected

times. The influence of subsidence is predicted to extend beyond the edge of the salt dome at West Hackberry, which varies from approximately 3000 to 8000 ft from the center of the cavern field (Magorian, et al, 1991).

The calculated surface strains at the above times is shown in Figure 13 for 20 years (prior to leaching) and after the 5th leach. In comparison to the allowable 1 millistrain, Section 2.7, the current day accumulated strain is below the limiting value and thus preventing structural damage. After the 5th leach, the strain is at 1.5 millistrains which is sufficient to cause mild structural damage. The damage results from compressive strains, and tensile strains, which can be characteristic of surface subsidence are not predicted.

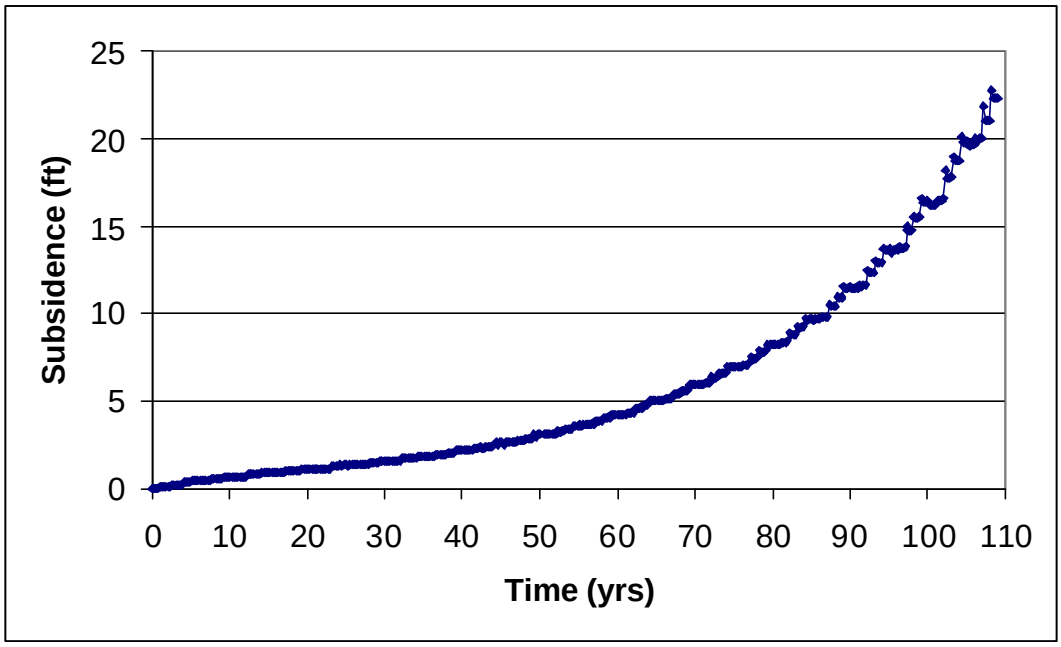

Figure 10. Subsidence at center of cavern field vs. time.

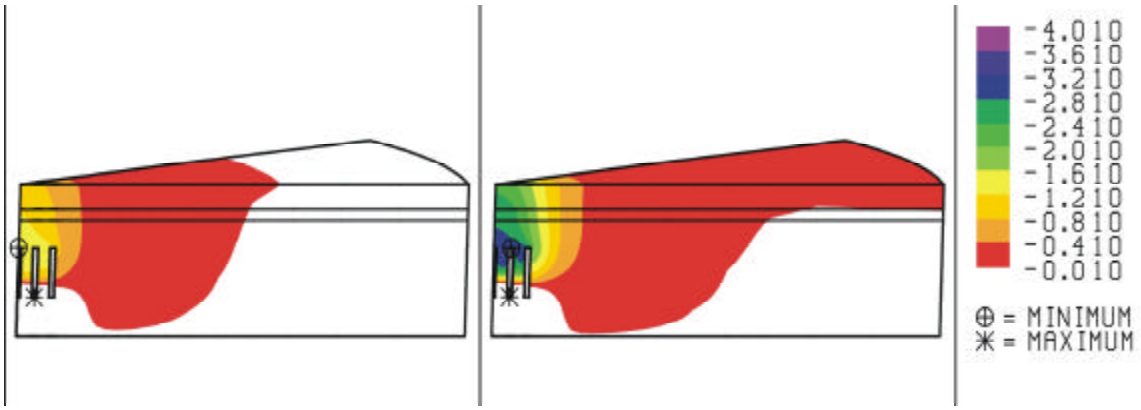

Figure 11. Vertical displacements (m) prior to leaching and immediately before 6th leach.

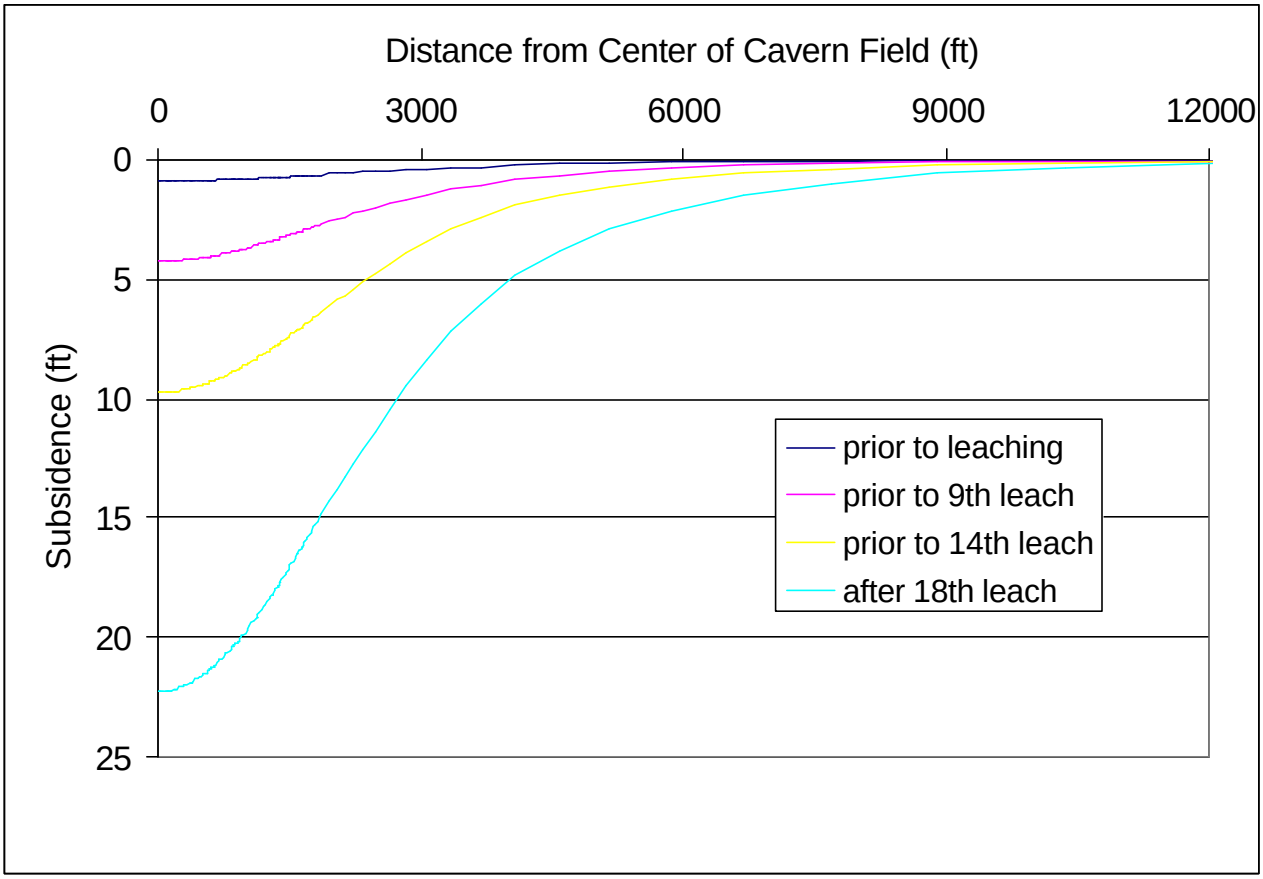

Figure 12. Subsidence profiles at surface over time.

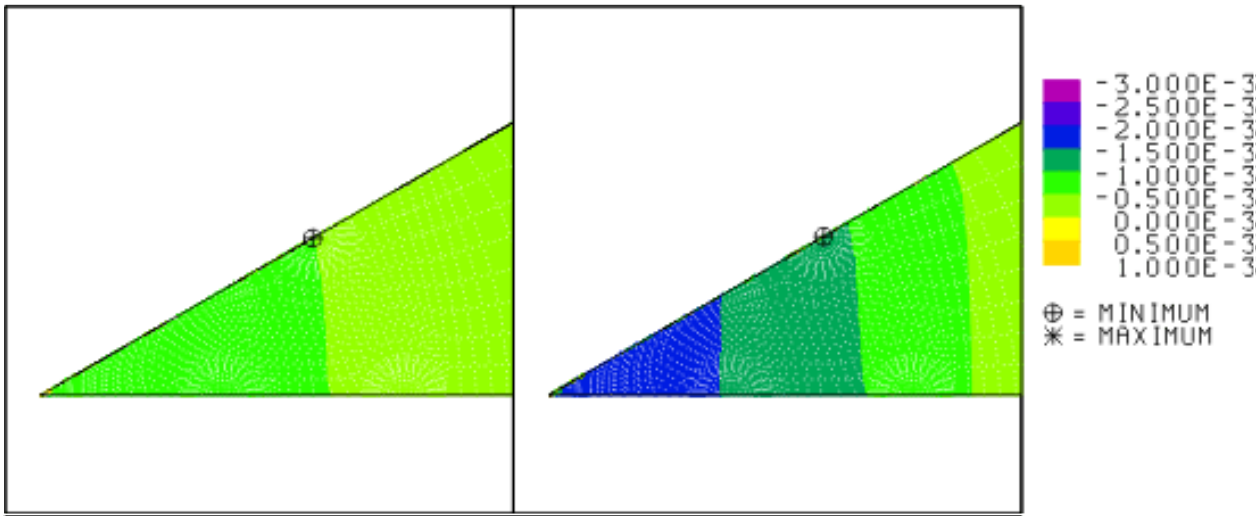

Figure 13. Predicted radial surface strains prior to leaching (20 years) and immediately before the 6th leach.

3.5 Cavern Wells

The predicted vertical strains are shown in Figure 14 at 20 years (prior to any leaching) and after the 5th leach. Of interest are the magnitudes in the location of the cavern wells. The allowable strain was estimated to be 0.2 millistrains in Section 2.7 for cement in tension. The strain criteria is exceeded at 20 years, which corresponds to the present time. The most vulnerable location for horizontal fracturing, as discussed before, is the caprock region due to corrosion considerations. This area shows the least ground strain, however the ground strains may be of sufficient magnitude (.2 to .4 millistrains) at 20 years to results in mild damage. Higher strains are found over the central portion of the cavern field, particularly directly above the cavern roofs and in the overburden. As discussed earlier, the physical presences of the wells is not simulated in this model, and thus any mitigating influence of the steel casing on the cement is not accounted for in these evaluations. The suggested ground strains thus call for a more detailed analysis prior to drawing strong conclusions.

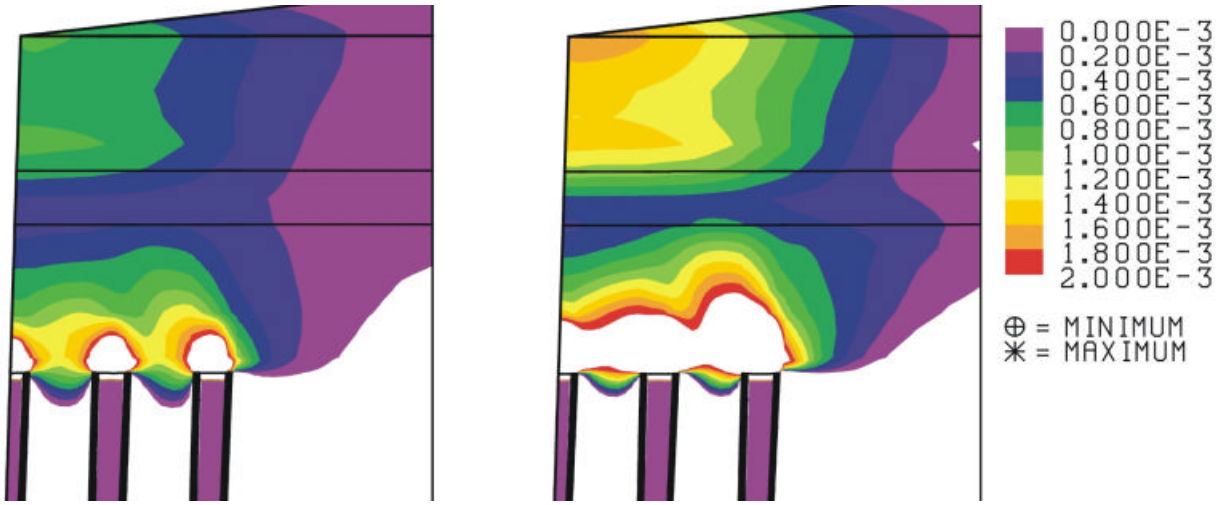

Figure 14. Vertical ground strains near cavern wells prior to and immediately before the 6th leach.

3.6 Cavern Stability

The stability of the caverns were evaluated by examination for any tensile stresses and calculation of the safety factor against dilatant damage. The greatest potential for failure occurred in the wall of the caverns immediately following the application of workover pressures. The worst location was predicted between caverns 2 and 4, when cavern 4 was being worked-over. For example, at 45 years, immediately prior to the 6^{h} leach, the response of cavern 4 to workover pressures is shown in Figure 15. A slight interaction is noted with neighboring cavern (no. 2), but the stresses do not compromise the stability of the salt web separating the caverns, until after the 15^{th} leach as shown in Figure 16. Tensile stresses were predicted to span the entire region between caverns 2 and 4 during that time, and the magnitude increase for subsequent leaches, thus assuring failure of salt between the caverns.

Examination of a typical distribution for safety factor against dilatant damage over the cavern surface is provided in Figure 17 for various times prior to the 5^{th} leach. The influence of workovers is noted by the drops in safety factor from 3.3 to approximately 2. The minimum safety factor is predicted at the wall of the caverns, near the roof. The minimum safety factor for damage is plotted in Figure 18 over time. Similar to the tensile damage, dilatancy is predicted to occur after 90 years (15^{th} leach) with failure at the 16^{th} leach. In the absence of workover pressures, the salt does not damage or fail throughout the duration of the analyses (18 leaches and 110 years).

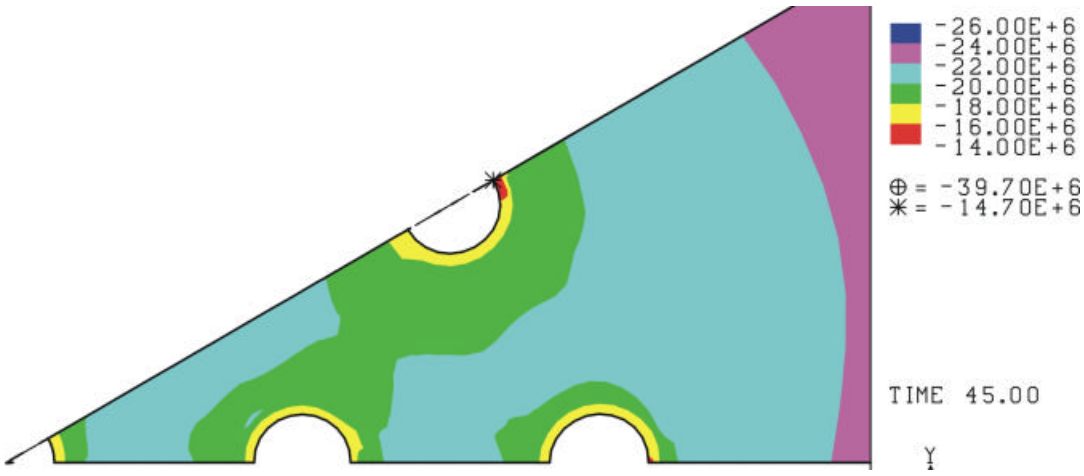

Figure 15. Least compressive stress (Pa) at 45 years. Horizontal cross-section at 600 ft above floor.

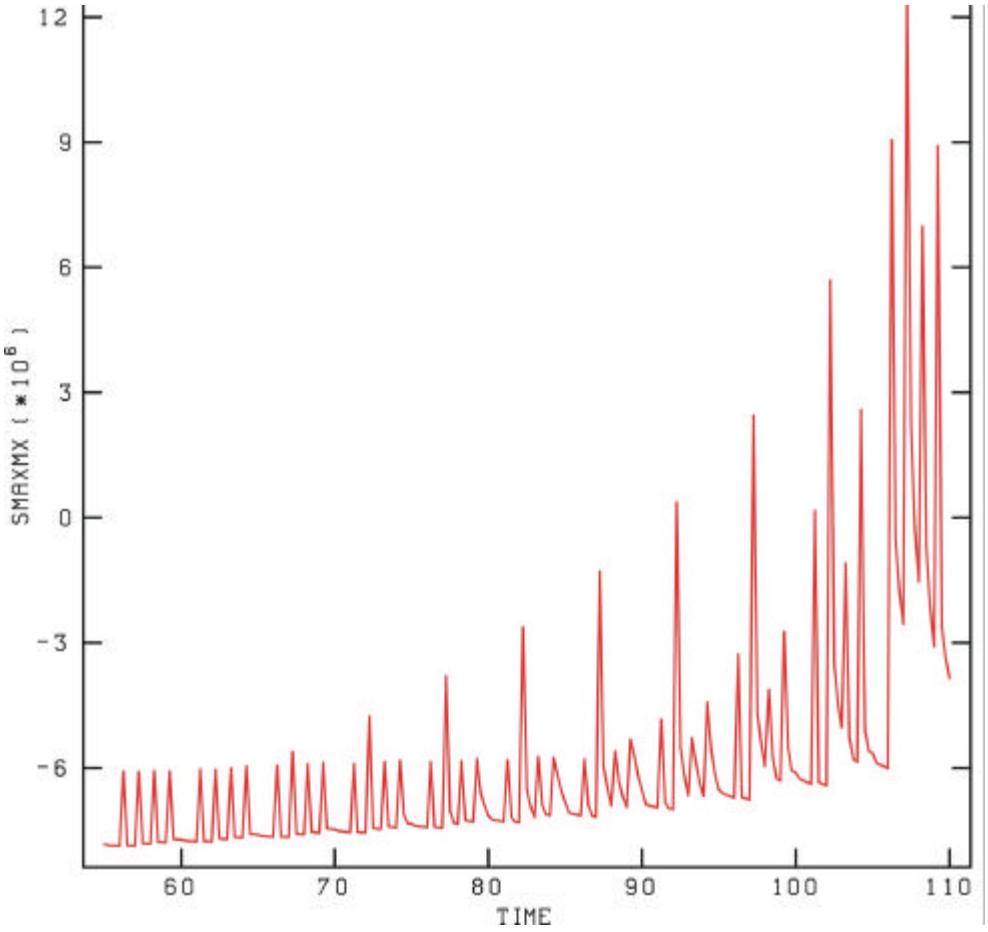

Figure 16. Minimum Compressive Stresses (Pa) vs. Time (tensile stresses are positive).

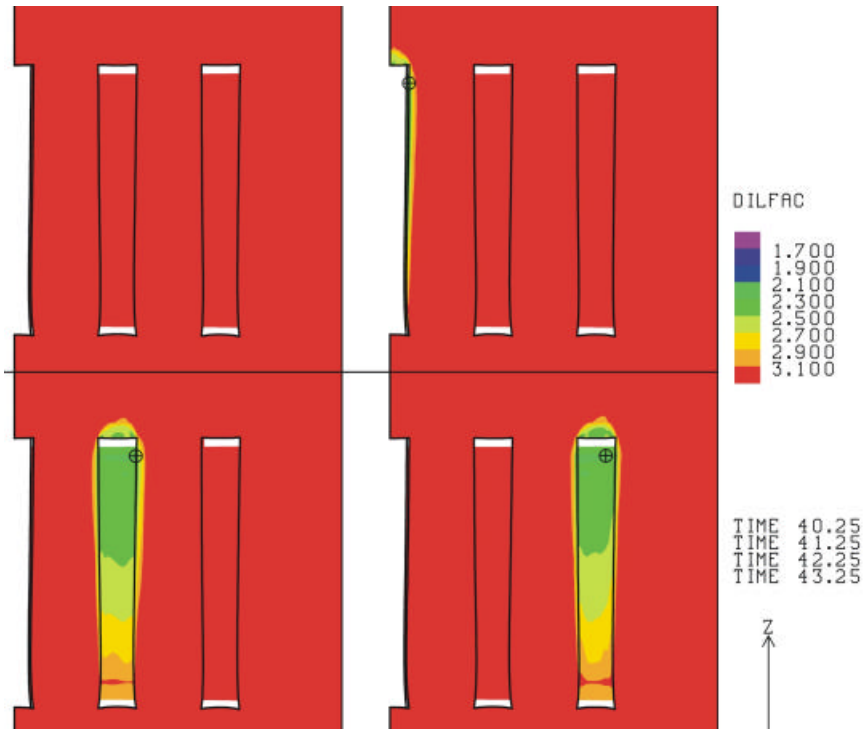

Figure 17. Safety factor contours for dilatant damage during workovers of each cavern before the 6th leach.

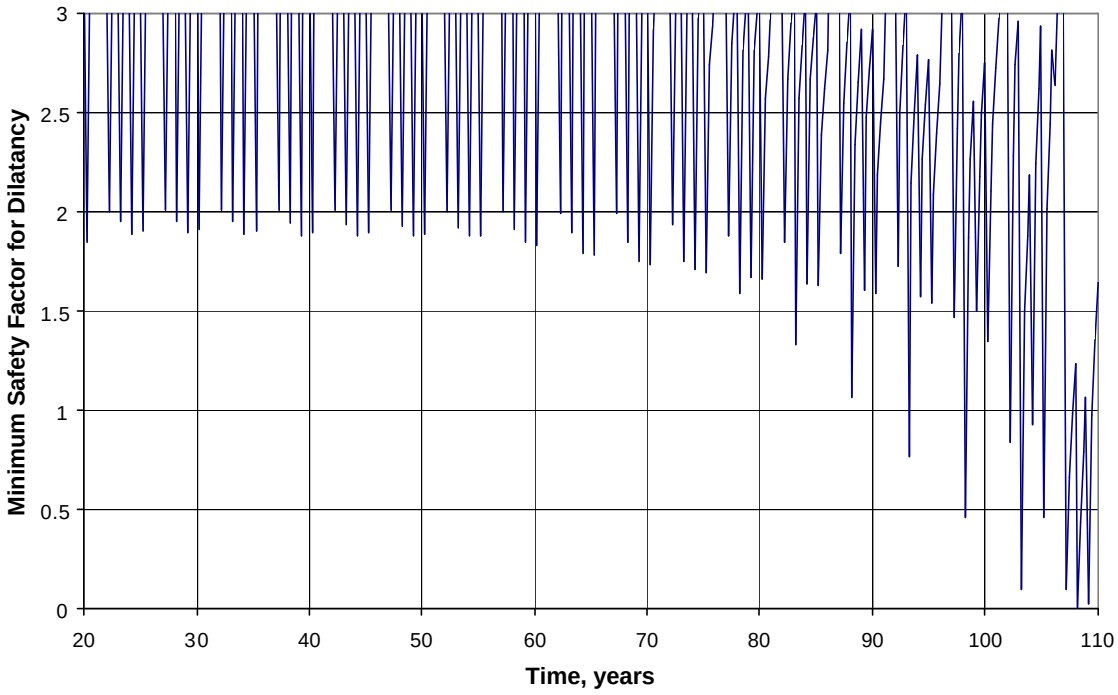

Figure 18. Minimum safety factor against dilatant damage.

4.0 Conclusions

3-D finite element analysis of a typical SPR cavern field quantified the geotechnical consequences associated with continued leaching caverns until caverns approached coalescence. The analyses used properties similar to those of the West Hackberry field in Louisiana and accurately predicted its behavior for the past 20 years. The excellent agreement between measured and predicted surface subsidences and cavern closures inferred through well head pressurization rates provide some confidence that the model predictions involving future cavern leaches are accurate, but the validation is tempered to date by the lack of a large scale oil drawdown to compare to.

The analyses predict that the caverns will remain stable well beyond the current 5 drawdowns. Damage is not predicted until the 15^{th} leach with failure occurring during the 16^{th} leach. The damage and failure occurs during workover conditions. In the absence of workovers, the caverns would remain stable. The strains imposed on the wells and surface structure were sufficient to cause damage to the wells and surface structure much earlier. Elongation of the wells, due to subsidence, resulted in vertical strains that currently approach the limit for cement. Additional straining may result in horizontal cracking, which may be of concern, particularly in the cap rock region, in that corrosive groundwater may gain access to the steel casings. The model does not account for the physical presence of the well or casings. Practically all SPR wells contain 2 cemented steel casings into the salt. Therefore the actual response of these wells is difficult to quantify with the simplistic well model used in this report, but the analyses do highlight the need for further evaluation.

The surface strains were of sufficient magnitude (approximately 1 millistrain) to cause slight damage to surface structures, based on allowable strains found in various country regulations, at about the 5^{th} drawdown. The specific location and design of structures will control the actual response along with the actual site operations. The analyses presented in this report assume a future of full site drawdowns spaced every 5 years. The subsidence rate, and hence magnitude of subsidence, is predicted to increase as cavern size increases. The relationship is largely controlled by cavern volume as the creep rate, as measured by percent closure, is not predicted to increase very much due to drawdowns. The additional subsidence will require some mitigative action to prevent flooding at some point. It is likely that the costs associated with the geotechnical consequences of enlarged caverns will increase with each drawdown.

The analyses presented in this report can be used as a guide. They suggests that some mitigative work may be required prior to extensive leaching of the caverns. Well strains already appear to be at limiting values, and surface strains could start to damage structures after a number of leaches. The impacts on cavern wells and surface structure can be mitigated through engineering, as can the potential for surface flooding due to subsidence. The integrity of the cavern, on the other hand, must be assured through proper operations. The analyses predict damage of the salt, but not until 15 leaches with significant failure after 16 leaches during workover conditions. The pillar width at the onset of damage was

approximately 220 ft, with a resulting P/D ratio of 0.4, which is well below the current criteria of 1.78.

References

Ballard, S. and B.L. Ehgartner. Caveman Version 3.0: A Software System for SPR Cavern Pressure Analysis. SAND2000-1751, Sandia National Laboratories, Albuquerque, New Mexico, July, 2000.

Bauer, S.J. West Hackberry Measurements completed November, 1998: Analysis and Comment. Letter report, Sandia National Laboratories, Albuquerque, New Mexico to J.C. Kilroy, January 22, 1999.

Blandford, M.L., JAS3D- A Multi-Strategy Iterative Code for Solid Mechanics Analysis: User's Instructions, Release 1.6, Sandia National Laboratories, Albuquerque, New Mexico, September 1998.

Ehgartner, B.L. Utilization of SPR Caverns- allowable number of drawdowns and P/D ratios, memo to J.K. Linn, Sandia National Laboratories, Albuquerque, New Mexico, February 25, 2000.

Hoffman, E.L. Investigation of Analysis Assumptions for SPR Calculations, memo to J. K. Linn, Sandia National Laboratories, Albuquerque, New Mexico, February 7, 1992.

Hoffman, E.L. and B.L. Ehgartner, Evaluating the Effects of the Number of Caverns on the Performance of Underground Oil Storage Facilities, Int. J. Mech. Min. Sci. & Geomechanics, Vol 30, No. 7, 1993.

Hoffman, E.L., Effects of Cavern Spacing on the Performance and Stability of Gas-Filled Storage Caverns, SAND92-2545, Sandia National Laboratories, Albuquerque, New Mexico, April, 1993.

Hunsche, U.E. "Failure Behavior of Rock Salt Around Underground Cavities," 7th International Symposium on Salt, 1992.

Krieg, R.D. Reference Stratigraphy and Rock Properties for the Waste Isolation Pilot Plant (WIPP) Project, SAND83- 1908, Sandia National Laboratories, Albuquerque, NM, January 1984.

Magorian, T.R., J.T. Neal, S. Perkins, Q.J. Xiao, and K.O. Bryne. Strategic Petroleum Reserve (SPR) Additional Geologic Site Characterization Studies West Hackberry Salt Dome. SAND90-0224, Sandia National Laboratories, Albuquerque, NM, January 1991.

Morgan, H. S. and R.D. Krieg. Investigation of an Empirical Creep Law for Rock Salt that Uses Reduced Elastic Moduli. 31st U.S. Symposium on Rock Mechanics, CO School of Mines, June 18-20, 1990.

Munson, D.E. Analysis of Multistage and Other Creep Data for Domal Salts, SAND98-2276, Sandia National Laboratories, Albuquerque, NM, January 1998.

Peng, S.S. Coal Mine Ground Control, 2nd Ed., John Wiley and Sons, New York NY, 1985.

Preece, D.S. and J. T. Foley. Long Term Performance Prediction for Strategic Petroleum Reserve (SPR) Salt Caverns. SAND83-2343, Sandia National Laboratories, Albuquerque, NM, December 1984.

Speirs, C.J., C. J. Peach, R.H. Brzesowsky, P.M.T.M. Schutjens, J. L. Liezenberg, and H.J. Zwart, "Long Term Rheological and Transport Properties of Dry and Wet Rocks, EUR 11848, prepared for Commission of the European Communities, by University of Utrecht, Utrecht, The Netherlands, 1988.

Tavares, M.P., Dilatancy and Failure Criteria for SPR Rock Salt. Internal Report to J.K. Linn, Sandia National Laboratories, Albuquerque, NM, August 9, 1994.

Thorton, C.H and I.P. Lew. Concrete and Design Construction. Standard Handbook for Civil Engineers, Chapter 8, 3rd ed., F.S. Merritt, editor, McGraw-Hill, NY, 1983.

Van Sambeek, L., J. Ratigan, and F. Hansen, Dilatancy of Rock Salt in Laboratory Tests, Proc. 34th U.S. Symposium on Rock Mechanics, 1993, 245-248

Wawersik, W.R. and D.H. Zeuch, Creep and Creep Modeling of Three Domal Salts- A Comprehensive Update, SAND84-0568, Sandia National Laboratories, May 1984.

DISTRIBUTION

U.S. DOE SPR PMO ( )
900 Commerce Road East
New Orleans, LA 70123
Attn: W. C. Gibson, FE 44
G. B. Berndsen, FE 443.1
J. Culbert, FE 443
W.S. Elias, FE-4431
J. C. Kilroy, FE 442
R. E. Myers, FE 4421
W. Poarch, FE 4421
TDCS (2)

U.S. Department of Energy ( )
Strategic Petroleum Reserve
1000 Independence Avenue SW
Washington, D.C. 20585
Attn: D. Johnson, FE 421

DynMcDermott ( )
850 South Clearview Parkway
New Orleans, LA 70123
Attn: J. A. Farquhar, DM 21
J. M. McHenry. DM-21

Sandia Internal:
MS 0701 P. J. Davies, 6100
MS 0741 M. Tatro, 6200
MS 0706 R. E. Finley, 6113
MS 0706 S. J. Bauer, 6113
MS 0706 B. L. Ehgartner, 6113 (10)
MS 0706 T. E. Hinkebein, 6113
MS 0706 B. L. Levin, 6113
MS 0706 M. A. Molecke, 6113
MS 0706 D. E. Munson, 6113
MS 0706 C. C. Rautman, 6113
MS 0706 A. R. Sattler, 6113
MS 0751 L. S. Costin, 6117
MS 0751 S. R. Sobolik, 6117 (3)
MS 0751 R.P. Jensen, 6117
MS 0719 W. Cox, 6131
MS 0718 K. Sorenson, 6141
MS 9018 Central Tech. Files, 8940-2
MS 0899 Technical Library, 9616 (2)
MS 0612 Review and Approval Desk
For DOE/OSTI, 9612